

Size effect on the melting temperature of gold particles*

Ph. Buffat and J-P. Borel

Laboratoire de Physique Experimentale, Ecole Polytechnique Fédérale-Lausanne, Lausanne, Switzerland

(Received 2 December 1975)

Recently, small particles have been shown to exhibit a melting temperature which depends on the particle size. The various possible experimental methods have been compared and measurements of the melting points of small gold particles have been made using a scanning electron-diffraction technique. This method was applied to particles having diameters down to 20 Å. Consideration of the size distribution over an entire sample makes it necessary to carry out a careful analysis of the experimental results in order to deduce the melting temperature of particles having a well-defined diameter. The experimental results are quantitatively in good agreement with two phenomenological models. The first model describes the equilibrium condition for a system formed by a solid particle, a liquid particle having the same mass, and their saturating vapor phase. The second model assumes the preexistence of a liquid layer surrounding the solid particle and describes the equilibrium of such a system in the presence of the vapor phase. In order to permit a better comparison between both models, a new expression for the thermodynamic equilibrium condition has been derived in the present work. In the case of the first model, the agreement was obtained using only the physical constants of massive gold. In applying the second model, however, one is compelled to assume the existence of a liquid layer having a thickness of about 6 Å.

I. INTRODUCTION

Between the dimensions on an atomic scale and the dimensions which characterize bulk material is to be found a size range where condensed matter exhibits some remarkable specific properties. We present here results which are related to an essentially thermodynamic size effect, i.e., the reduction of the melting point of small gold aggregates as a function of decreasing particle size. For the range of particle sizes greater than 50 Å, some similar experimental investigations have been performed previously on various substances, and the results of these investigations have been generally in agreement with the various phenomenological models which have been proposed to account for this effect.

In the present work, we have employed a scanning electron-diffraction technique to extend the measurements to include particle sizes in the range between 50 and 20 Å. It should be noted that this technique is not applicable in the case of particles whose size is less than 20 Å. Additionally, the same phenomenological approach cannot be used to predict any definite melting point for these very small particles since the very small particles begin to adopt the specific forms associated with clusters.^{1,2}

In the present work a decision was made to investigate small particles of gold for two principal reasons: First, gold has a very weak affinity for oxygen, and second, the vapor pressure of gold remains relatively low up to the melting point. The latter property is particularly important in order to prevent the occurrence of significant

changes in the sample dimensions by evaporation during the course of the experiment.

Although it is only possible to formulate a valid theoretical description of the melting point of the thermodynamic limit (i.e., for those systems whose dimensions are infinite), nevertheless, it is possible to define the melting temperature of a small system in the sense that it is possible to make an experimental determination of this temperature. Three different criteria could be used for this determination: (i) the disappearance of the state of order in the solid; (ii) the sharp variation of some physical properties: evaporation rate, magnetic susceptibility, etc.; (iii) the sudden change in the particle shape.

Several observations of the melting point of small particles have been made previously using the above criteria, and this work will be described in Sec. II. In Sec. III the question of the melting point of small particles will be discussed from a phenomenological standpoint, and an extension of one of the existing models will be proposed. In Secs. IV–VI the present investigation will be described. Finally, in Secs. VII and VIII our results will be compared with the theoretical predictions.

II. OBSERVATIONAL METHODS

A. Disappearance of the state of order in the solid

The diffraction of high-energy electrons by crystalline powders produces patterns of rings that are relatively narrow compared to those obtained from electron diffraction by liquids. Accordingly, by using a heated (or cooled) stage in either an electron diffractometer or an electron

microscope, it is possible to determine the temperature at which the morphological change of the rings occurs and, thereby, to determine the melting temperature of the very small crystals. This method is well suited to particles whose diameter is greater than 20 Å, however. Because of the dispersion of sizes of crystals encountered in a specimen, it is generally not possible to observe a sharp change in the ring patterns during the melting process. Therefore, this method only permits the determination of a range of melting temperatures for an ensemble of particle sizes. The technique would, of course, be well suited to the study of a set of particles with identical diameters. Despite this limitation, it was possible to utilize this method in the present work by taking into account the size distribution of the particles and by making quantitative studies of the morphological changes of the diffraction rings.

The diffraction technique was first used by Takagi³ in the study of Pb, Sn, and Bi. Later, Blackman *et al.*⁴ investigated Sn; Wronski,⁵ Sn; Coombes,⁶ Pb and In; and Gladkich *et al.*,⁷ Ag, Cu, Al, and Ge. Additionally Boiko *et al.*⁸ have investigated indium. An attempt to improve the technique by restricting the diffracting area of the sample in an electron microscope was also made by Poczka *et al.*⁹ By heating a sample of indium, they were able to determine the temperature at which the last diffracted beam characteristic of a solid structure disappeared, and they related this temperature to the melting point of the most massive crystal in the field of observation. Using a closely related approach, Berman *et al.*¹⁰ have studied indium crystals by dark-field electron microscopy. With this technique, only those crystals which diffract in the direction of the objective diaphragm are observed. The image of the crystal naturally disappears when the melting point is reached. Implicit in the accuracy of this technique is the assumption that the orientations of the crystals do not change either as a result of crystalline reordering or by deformations in the substrate as the temperature is varied. This method has the advantage of allowing measurements to be made on individual particles, but its applicability could be impaired as a result of heating of the sample by the electron beam, since the current density applied in this technique may be several orders of magnitude higher than that used in ordinary electron diffraction. The fact that the heating of the sample in numerous electron microscopes (e.g., the Philips EM 300) is achieved by conduction and not by thermal radiation also limits this technique to temperatures which are relatively close to room temperature in order to avoid large uncertainties in the measurement of the actual

temperature of the particles. Other measurements of the melting point of small particles which are of interest have been made by Petrov using x-ray diffraction techniques on particles of Pb, Bi, and Ag which were dispersed in a varnish.¹¹

B. Modification of the rate of evaporation at the melting point

In observing the evolution of small gold crystals by electron microscopy at a constant temperature, Sambles¹² noticed that the rate of evaporation underwent a sharp increase at a temperature which was slightly below the melting temperature of the bulk material. He assigned this increase in the evaporation rate to a variation of the evaporation coefficient which occurred during the melting of those crystals which had been brought to the melting point by evaporation. As a result of the heating induced by the electron beam and due to the heat loss by thermal radiation, there is an uncertainty in the correlation between the furnace temperature and the actual temperature of the crystals. Therefore Sambles used the rate of evaporation to determine the temperature, and took advantage of his former investigations on the Kelvin law (effect of the size of the vapor pressure of the liquid¹³).

This technique is well suited to metals which have a vapor pressure of about 10⁻⁵ Torr at the melting point, and which, therefore, evaporate at the proper rate. The applicability of this technique is, however, limited to particles with relatively large sizes since its use requires the precise measurement of the size variations during the process.

C. Modification of the particle shape at the melting point

Samples of Bi and Pb have been studied by Peppiatt,¹⁴ and Blackman *et al.*,¹⁵ who attributed the transition from polyhedral to spherical shapes undergone by some crystals to an effect associated with the melting of the solid. Their method was to submit the sample to alternate isothermal annealings without the electron beam and to perform the observations at a lower temperature. As a result of superfusion, they noted that the particles melted in the course of successive annealings and remained so during the observation. This method avoided the heating of the sample by the electron beam and offered the advantage of studying individual particles. The technique can be applied, however, only to those crystals which clearly exhibit a pronounced polyhedral shape (i.e., to crystals about 200 Å or greater in diameter).

A method similar to that used by Peppiatt has been employed by Sundquist¹⁶ to investigate the possibility of a surface-roughness phenomenon.

Unfortunately, however, the occurrence of adsorption enhances the faceting of the crystals and makes a study of this type quite difficult.^{17,18}

III. PHENOMENOLOGY

One can attempt to apply the known methods of phenomenological thermodynamics to systems of finite size by introducing the Gibbs model to account for the existence of a surface. For a crystal obeying the Curie-Wulff relationship $\gamma_i/h_i = Ct$ (where γ_i is the surfact tension of the i th face and h_i is the distance from this face to a given point) one finds as a first approximation that the chemical potential is modified by the presence of an additive term given by $2\gamma_i/\rho h_i$, where ρ is the specific gravity.¹⁹ The modification undergone by the chemical potential implies a parallel modification of the chemical and physical properties of the material. An example of such a modification is given by the vapor pressure of metallic particles of the order of 100 Å. The vapor pressure of such particles is notably higher than that of the bulk material.^{13,20-22} A dependence of the temperature of the melting point on the particle size should also be expected. Several authors have attempted to predict a dependence of this type using a thermodynamic approach, and from this work the following two main models have emerged:

(i) First the starting assumption is made of the simultaneous existence of a solid particle, of a liquid particle having the same mass, and of a vapor phase. The equilibrium conditions are then described based on these assumptions.²³⁻²⁵

(ii) The solid particle is considered as being embedded in a thin molten layer and the behavior of the whole ensemble is described using the thickness of the liquid layer as a parameter whose value may be adjusted in accordance with the experimental results.^{5,6,26}

As a first approximation, Pawlow has shown that the first model noted above leads to a linear relationship between the relative lowering of the melting temperature and the surface curvature of the particles.²³ The second model is more closely associated with the experimental results since it includes terms which are nonlinear with respect to the surface curvature. Figure 1 shows the predictions which can be drawn from both the two phenomenological models and the physical constants of gold which can be found in the literature (see Table I).

In the present work, we have extended the results of Pawlow by considering a higher-order approximation which permits a better comparison to be made for both models. This extension proceeds along the lines of a previously described calculation.²⁵ First, we consider a solid or a liquid par-

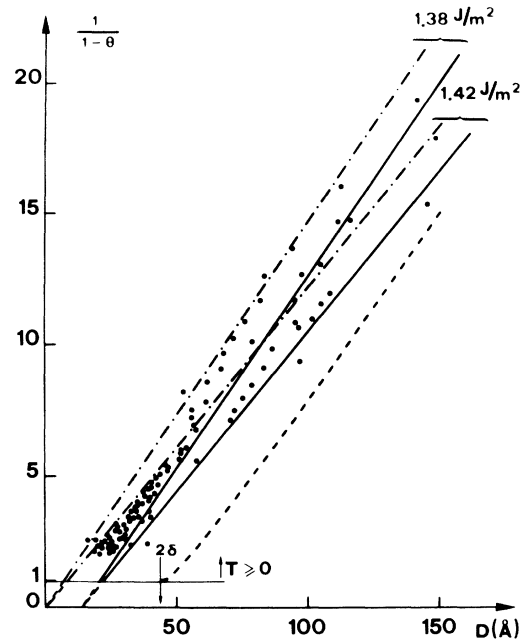


FIG. 1. Experimental and theoretical values of $(1 - \Theta)^{-1}$ vs particle diameters. In the case of the first model, two published values of gold surface tension were used to draw corresponding pairs of theoretical predictions: filled circles, present experimental work; dashed-and-dotted lines, first model and first-order approximation [Eq. (14)]; solid lines, first model and second-order approximation [Eq. (13)]; dashed line, second model [Eq. (18)].

title. The volume contribution to the chemical potential characterizing this particle can be written in any case as the following power series:

$$\begin{aligned} \mu(T, P) = & \mu(T_0, P_0) + \frac{\partial \mu}{\partial T} (T - T_0) + \frac{\partial \mu}{\partial P} (P - P_0) \\ & + \frac{\partial^2 \mu}{\partial T^2} \frac{(T - T_0)^2}{2} + \frac{\partial^2 \mu}{\partial P^2} \frac{(P - P_0)^2}{2} \\ & + \frac{\partial^2 \mu}{\partial P \partial T} (P - P_0)(T - T_0) + \dots \end{aligned} \quad (1)$$

In the treatment that follows we will restrict our considerations to second-order terms. The Gibbs-Duhem relationship given by the expression

$$-V dp + S dT + m d\mu = 0 \quad (2)$$

will be used to calculate the coefficients of the preceding development. Using the Gibbs-Duhem relationship, we may write the following equations:

$$\frac{\partial \mu}{\partial T} = -\frac{S}{m} = -s, \quad (3)$$

where s is the entropy per unit mass;

$$\frac{\partial \mu}{\partial P} = \frac{V}{m} = \frac{1}{\rho}, \quad (4)$$

where ρ is the density;

$$\frac{\partial^2 \mu}{\partial P^2} = -\frac{1}{\rho^2} \frac{\partial \rho}{\partial P} = -\frac{\chi}{\rho}, \quad (5)$$

where χ is the isothermal compressibility coefficient;

$$\frac{\partial^2 \mu}{\partial T^2} = -\frac{\partial s}{\partial T} = -\frac{C_p}{T}, \quad (6)$$

where C_p is the specific heat at constant pressure; and

$$\frac{\partial^2 \mu}{\partial P \partial T} = -\frac{1}{\rho^2} \frac{\partial \rho}{\partial T} \approx \frac{3\alpha}{\rho}, \quad (7)$$

where α is the linear-expansion coefficient.

If we refer to the liquid and solid parts by using the subscripts l and s , the equilibrium equation $\mu_l = \mu_s$ now may be written as

$$0 = \mu_l(T_0, P_0) - \mu_s(T_0, P_0) + (s_l - s_s)(T - T_0) + \frac{(P_l - P_0)}{\rho_l} - \frac{(P_s - P_0)}{\rho_s} - \frac{C_{pl} - C_{ps}}{2T_0}(T - T_0)^2 - \frac{\chi_l}{2\rho_l}(P_l - P_0)^2 + \frac{\chi_s}{2\rho_s}(P_s - P_0)^2 + 3 \left[\frac{\alpha_l}{\rho_l}(P_l - P_0) - \frac{\alpha_s}{\rho_s}(P_s - P_0) \right] (T - T_0). \quad (8)$$

The quantities s , ρ , α , C_p , and χ are taken at temperature T_0 and at pressure P_0 . Both T_0 and P_0 can be chosen so that they correspond, respectively, to the temperature and pressure associated with the triple point of the bulk phases. We can now write the expression $\mu_l(T_0, P_0) = \mu_s(T_0, P_0)$ and use the equilibrium equation to calculate the quantity $\Theta = T/T_0$, which is a measure of the relative lowering of the melting point.

The pressure P_l in a droplet is given by the Laplace law,

$$P_l = P_{\text{ext}} + 2\gamma_l/r_l, \quad (9)$$

where r_l is the radius of the droplet and P_{ext} is the pressure in the gaseous phase. For small systems, P_{ext} may be neglected since $P_l \gg P_{\text{ext}}$. The pressure P_l may also be related to the ratio γ_l/r_l at the temperature T_0 by writing the equation

$$\frac{\gamma_l}{r_l} \Big|_T = \frac{\gamma_l}{r_l} \Big|_{T_0} [1 - (\eta_l + \alpha_l)(T - T_0)], \quad (10)$$

where $\eta_l = -(1/\gamma_l)\partial\gamma_l/\partial T$ expresses the relative slope of the so-called Eötvös straight line.

In the case of the Curie-Wulff crystal, Defay *et al.*¹⁹ have shown that it is possible in a strictly formal sense to introduce an equivalent pressure P_s given by

$$P_s = P_{\text{ext}} + 2\gamma_s/h_s. \quad (11)$$

It is still necessary to have the latent heat of fusion $L = (s_l - s_s)T_0$ and the geometrical relationship given by the equation

$$r_s = (\rho_l/\rho_s)^{1/3} r_l, \quad (12)$$

which is valid for small particles with spherical shape. (γ_s will be used to denote the surface tension of the solid.) The question of the shape of the solid particles and of the value of γ_s will be treated in a following discussion.

The equilibrium condition can now be written as:

$$0 = L(1 - \Theta) - \frac{2}{\rho_s r_s} \left[\gamma_s - \gamma_l \left(\frac{\rho_s}{\rho_l} \right)^{2/3} \right] + \frac{C_{ps} - C_{pl}}{2} T_0 (1 - \Theta)^2 - \frac{2}{\rho_s r_s} \left[\gamma_s (\eta_s - 2\alpha_s) - \gamma_l (\eta_l - 2\alpha_l) \left(\frac{\rho_s}{\rho_l} \right)^{2/3} \right] T_0 (1 - \Theta) + \frac{2}{\rho_s r_s^2} \left[\chi_s \gamma_s^2 - \chi_l \gamma_l^2 \left(\frac{\rho_s}{\rho_l} \right)^{1/3} \right]. \quad (13)$$

Neglecting the second-order terms in the above equation, one obtains the well-known equation²⁴

$$1 - \Theta = \frac{2}{\rho_s L r_s} \left[\gamma_s - \gamma_l \left(\frac{\rho_s}{\rho_l} \right)^{2/3} \right]. \quad (14)$$

The above approximations will be discussed later and compared with the experimental results (Figs. 5-7).

The second equilibrium condition $\mu_s = \mu_g$ allows us to obtain an expression for the pressure in the

gaseous phase (saturating vapor pressure). As a first-order approximation, this leads, of course, to the Gibbs-Thomson relationship.²⁷

It should be noted that the function $\ln\Theta$ is sometimes employed by some authors instead of the term $(\Theta - 1)$. This logarithmic dependence could also be obtained using our approach by employing the Clapeyron equation

$$\frac{dL}{dT} = \frac{L}{T} + C_l - C_s \quad (15)$$

instead of the partial derivative

$$\left(\frac{\partial L}{\partial T}\right)_p = C_l - C_s, \quad (16)$$

Such an exchange would not be exactly correct in this case.

In the development of the second phenomenological model, Wronski⁵ and Coombes⁶ have established the following relationship:

$$1 - \Theta = \frac{2}{\rho_s L} \left[\frac{\gamma_{sl}}{r - \delta} + \frac{\gamma_l}{r} \left(1 - \frac{\rho_s}{\rho_l} \right) \right], \quad (17)$$

where δ stands for the liquid-layer thickness, γ_{sl} for the solid-liquid interfacial tension, and r for the total radius of the particle at a temperature close to its melting point. Later Sambles²⁸ used this result to derive the following equation:

$$\ln \Theta = - \frac{2}{\rho_s L} \left(\frac{\rho_l}{\rho_s} \right)^{1/3} \times \frac{1}{r_s^*} \left\{ \gamma_l \left(1 - \frac{\rho_s}{\rho_l} \right) + \gamma_{sl} \left[1 - \frac{\delta}{r_s^*} \left(\frac{\rho_s}{\rho_l} \right)^{1/3} \right]^{-1} \right\}, \quad (18)$$

where r_s^* denotes the radius which would characterize the particle at its melting point assuming that it remained entirely in the solid form. These expressions naturally do not take into account the surface tension of the solid phase.

IV. EXPERIMENTAL

In the present investigation a specially modified Balzers KD4 electron diffractometer has been employed. The vacuum was maintained at a pressure below 2×10^{-6} Torr throughout the entire experiment. The pressure was measured in the vicinity of the sample by a hot-cathode ionization gauge. Additionally, the sample holder was surrounded by a copper cage which was cooled with liquid nitrogen.

The sample was formed by the condensation of gold vapor on a thin amorphous carbon film mounted on a gold mesh of the type used for electron microscopy. The furnace which formed the sample holder was made from graphite with spectroscopic purity (see Fig. 2). This material was selected because of its low affinity for gold. Additionally, the carbon microstructure helps to prevent the seizing of parts even after firing in a vacuum. In order to avoid deflections of the electron beam by spurious magnetic fields, an electron bombardment technique was used to heat the furnace. The cathode was formed by a tantalum wire which was maintained at a high temperature by a constant current. This wire was wound around the furnace in a manner which minimized the associated mag-

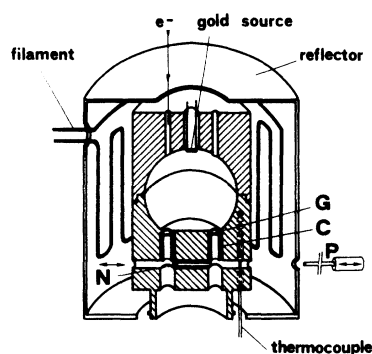


FIG. 2. Schematic of the furnace. Heating is achieved by electron bombardment. G, gold samples; C, cylinders; N, rod to maintain both cylinders C in position; P, pushing tool acting on rod N.

netic field.

The temperature measurements were made with a Pt-PtRh 10% thermocouple with 0.1-mm-diam wires. Since it was mandatory to ensure good thermal contact between the furnace and the thermocouple junction, the junction was formed in the shape of a disk with a diameter of 2 mm and a thickness of about 0.2 mm to give the best area/volume ratio.²⁹ A control experiment on the melting temperature of massive gold metal in this system resulted in a determination of the melting temperature of between 1335 and 1341 °K.

The electron-beam current was approximately 5×10^{-10} A and the accelerating voltage was 50 kV. At the sample position, the beam diameter was 0.3 mm. Assuming that thermal equilibrium results from radiation and that the total emissivity of gold is 0.03 at 800 °K,³⁰ it is possible to calculate that, at this temperature, a 1% absorption of the beam power would produce an increase of about 0.25 °K in the sample temperature.

The crucible used for the evaporation of the high-purity gold (99.9995%) consisted of a 0.8-mm diam molybdenum wire formed to approximate a plane source. By orienting the plane area tangentially to the spherical cavity of the furnace, and provided that the evaporation rate follows a cosine law with respect to the perpendicular to the crucible surface, we can assume that the inner walls of the furnace are also covered with gold crystals whose dimensions are close to those of the sample. Since the emission solid angle of the furnace is about $4\pi \times 10^{-2}$ sr, the particles are presumably in a near-equilibrium state with their vapor.

In order to determine possible morphological changes in the samples during the course of an experiment, the furnace contains two equivalent samples which can be extracted at any time without breaking the vacuum in the experimental cham-

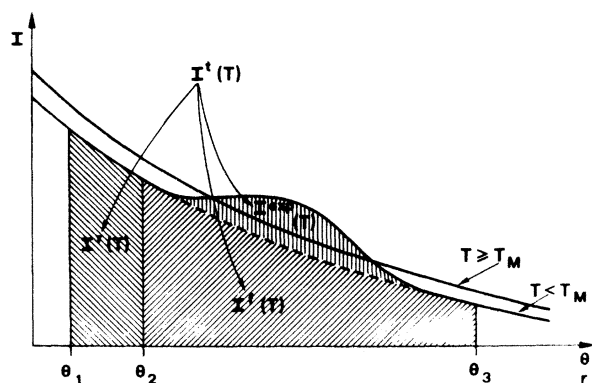


FIG. 3. Geometrical definition of the integrated intensities used in the vicinity of the (220) ring. $I^r(T)$ and $I^f(T)$ are both integrated intensities of the continuous background, respectively, between θ_1 and θ_2 , and between θ_2 and θ_3 . $I^{\text{exp}}(T)$ is the integrated intensity associated to the (220) ring. $I^t(T)$ is the total integrated intensity between θ_1 and θ_3 .

ber. As shown in Fig. 2, this is accomplished by fixing the two sample grids on two cylinders C which are partly overlaying and held in position by the rod N. A pushing tool P, which is normally located outside the diffractometer in order to move the rod N further into its housing, thereby allowing one of the two samples to fall into a small receiving vessel (not shown on this schematic).

The diffraction pattern can be analyzed at two locations using two detectors each of which is composed of an analyzing slit, a plastic scintillator sensitive to low-energy β 's, and a photomultiplier.

The signals from the photomultipliers were processed by a lock-in detection system. A plane condenser was mounted between the electron gun and the condenser of the illuminating system in order to modulate the signal. A square-wave voltage across the plane condenser provided for chopping the beam at the reference frequency. A second plane condenser was located next to the bottom of the furnace in order to deflect the diffracted beams. A ramp voltage was applied to this condenser to provide for a sequential analysis of the radial distribution of the intensity diffracted into an angular range of 6×10^{-3} rad. The resulting data were collected in a digitized form and were processed with an on-line minicomputer. This procedure gave direct access to the intensities $I^r(T)$ and $I^f(T)$ as defined in Fig. 3. These values along with the corresponding temperature were simultaneously punched for a later analysis.

The diffracted intensities were measured on the (220) ring since this is the most intense ring on

which the liquid-associated rings are not superimposed. Additionally the kinematic theory is more applicable to this ring than to, for example, the (111) ring. The sensitivity of the detection apparatus enabled us to follow the evolution of this ring for samples whose most probable diameter was as small as 25 Å.

V. PROCEDURE

To eliminate any vestiges of the previous experiment a preliminary heating of the furnace at temperatures up to above 1400 °K was first carried out. After the system had cooled, the vacuum was broken and the two sample meshes were mounted along with their holders. When the pressure in the sample chamber had been reduced below 2×10^{-6} Torr, the system was again heated to temperatures between 450 and 700 °K. This procedure permitted us to control the number of nucleation centers. A substrate temperature of between 300 and 450 °K was chosen, and the operation of evaporating the gold on the substrate was accomplished in about 5 sec.

Following the above procedure the sample is heated to a temperature slightly above the melting point of the largest constituent crystals. The size distribution of the entire set of crystals is then essentially invariant with respect to subsequent melting annealings. The cooling speed (7 min from 1100 to 700 °K) is sufficiently slow to allow equilibrium to be established over the entire sample. One of the samples is then preserved for a subsequent analysis of the size distribution. A second melting then takes place with the heating rate slower than 0.7 °K/sec. During this melting, both the temperature and the intensities diffracted in the (220) ring are recorded simultaneously by the digital data collection system and by analog means. The temperature is finally increased until it is no longer possible to distinguish the (220) ring on the analog recording, and the fusion is then considered to be complete. Control tests have shown that this process, when repeated on the same sample, gives results which are reproducible apart from slight effects due to evaporation.

After the sample has solidified, it is cooled to room temperature and is examined with a high-resolution Philips EM 300 S electron microscope which has been calibrated with a ruled grating (Fullam, 2160 lines/mm). The same cycle of operations is repeated during the photographic procedure in order to avoid different hysteresis effects in the microscope lenses. The size distribution is obtained from 5000 to 20 000 particles using a quantitative image analyzer (Quantimet 720, Metals Research) on the micrographs.

VI. DATA PROCESSING

During the course of an annealing which brings all of the particles above their melting temperature, changes can occur in the background intensity of the diffracted pattern. This effect has been accounted for in analyzing our results by explicitly assuming that the observed continuous background changes are related to amplitude changes and do not affect the angular distribution (see Fig. 3). The angular ring width under observation in these investigations appears small enough ($\Delta\theta = \pm 0.16\theta_{220}$) to justify this assumption.

By labeling $I^r(T)$ as the intensity of the reference continuous background measured outside of the diffracted ring (between θ_1 and θ_2), $I^f(T)$ as the intensity of the continuous background between θ_2 and θ_3 , $I^t(T)$ as the sum of the scattered and diffracted intensities measured between θ_1 and θ_3 , T_M as the uppermost temperature associated with the disappearance of the (220) ring, and since $I^{\text{exp}}(T_M) = 0$, we can write the following expressions:

$$I^f(T) = \frac{[I^t(T_M) - I^r(T_M)]I^r(T)}{I^r(T_M)}, \quad (19)$$

$$I^{\text{exp}}(T) = I^t(T) - I^r(T) \left[\frac{I^t(T_M)}{I^r(T_M)} \right]. \quad (20)$$

The evolution of $I^{\text{exp}}(T)$ with the temperature follows the Debye-Waller factor³¹ predictions as long as the last temperature is below the lowest melting temperature encountered in the sample:

$$I^{\text{exp}}(T) = I_0 e^{-2M} = I_0 \exp\left(-16\pi^2 \langle \mu^2 \rangle \frac{\sin^2 \theta_B}{\lambda^2}\right), \quad (21)$$

where $\langle \mu^2 \rangle$ is the mean-square displacement of the atoms in a direction perpendicular to the Bragg planes diffracting under θ_B , λ is the electron wavelength, and I_0 is the intensity at 0°K. We have assumed $\langle \mu^2 \rangle$ to be proportional to the temperature T , as it would be the case of the Debye model with T much greater than the Debye temperature. The experimental behavior of $I^{\text{exp}}(T)$ with respect to temperature is shown schematically in Fig. 4. As expected this variation exhibits an exponential decrease which corresponds to a single Debye-Waller factor followed by an even sharper decrease associated with fusion.

Since the small size of the particles enables us to utilize the results of the kinematic theory of electron diffraction,³² the integrated intensity diffracted by a family of planes is proportional to the total mass of the sample located in the beam. This result can be expressed by the equation

$$I^{\text{exp}}(T)/I^*(T) = M^{\text{sol}}(T)/M^{\text{tot}}, \quad (22)$$

where $I^{\text{exp}}(T)$ is the experimentally measured integrated intensity, $I^*(T)$ is the integrated intensity

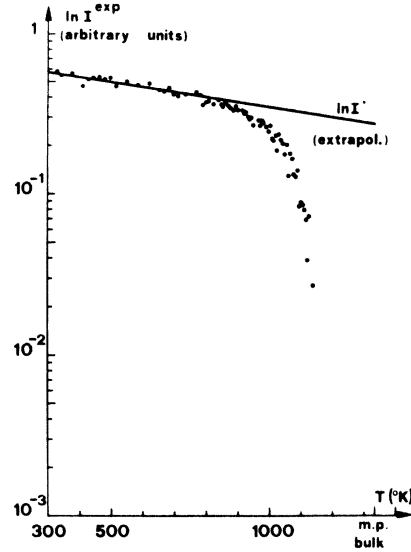


FIG. 4. Plot of the (220)-ring integrated intensity $I^{\text{exp}}(T)$ vs temperature. $I^*(T)$ is the integrated intensity derived from an extrapolation of those values of $I^{\text{exp}}(T)$ not directly associated with the melting process.

extrapolated as if fusion had not occurred, $M^{\text{sol}}(T)$ is the mass of all the crystals still in solid form under the beam, and M^{tot} is the mass of all the particles under the beam. The quantitative analysis performed with the electron microscope and the Quantimet system gives access to the mass distribution in the sample on the basis of particle size. The particle shapes in the present investigation appear to be quasispherical as determined by electron microscopy. This enables us to calculate $M^{\text{sol}}(T)$ using the equation

$$M^{\text{sol}}(T) = \rho_s \int_{D_m(T)}^{D_{\text{max}}} \frac{\pi}{6} D^3 dN(D), \quad (23)$$

where D_{max} is the diameter of the largest crystal encountered, $D_m(T)$ is a diameter below which all the particles are molten and above which all of the particles are still in solid form, $dN(D)$ is the number of particles having the diameter D as calculated by linear interpolation of the distribution determined using the Quantimet system, and ρ_s is the specific gravity of gold, whose variation with crystal size is neglected.^{33,34}

Thus an extrapolation of the linear part of $\ln I^{\text{exp}}(T)$ in the melting range provides the values of $I^{\text{exp}}(T)/I^*(T)$ in Eq. (22) and the relative mass distribution of solid particles $M^{\text{sol}}(T)/M^{\text{tot}}$ gives the diameter D_m of those crystals which just reach the melting point at the temperature T . Implicit in this determination is the assumption that each size is associated with one single melting temper-

ature. This temperature is then defined as the melting temperature of crystals having the size D_m .

VII. EXPERIMENTAL RESULTS

The integrated intensities $I^{\text{exp}}(T)$ have been computed for various sample temperatures using the measured diffracted intensities $I^r(T)$ and $I^t(T)$ and the computational procedure described previously.^{29,35} Curves similar to those illustrated in Fig. 4 have been obtained for each of the 22 samples that we investigated. At low temperature, the behavior of $\ln I^{\text{exp}}(T)$ is quite linear. This suggests that the Debye-Waller factor is only weakly dependent on the crystal size at least for the range of sizes encountered in each of our samples.

A. Comparison of results with the first phenomenological model

A least-squares fit to the straight portion of $\ln I^*(T)$ was used to determine the parameters appropriate to the linear range of behavior. In making this fit, all the values of $\ln I^{\text{exp}}(T)$ for temperatures below a limit which was estimated for each sample were taken into account. The residual portion of particles which are still solid and the size of those particles which are just reaching the melting point can now be obtained for each temperature at which a measurement is made by using Eq. (22). Points were considered relevant if at least 10% and at most 85% of the total mass of the sample was melted. Outside of this range, errors made in determining the slope of $\ln I^*(T)$, in the continuous background correction, or on the tails of the size distributions, could lead to substantial uncertainties in the size of the crystals which were in the process of melting.

Part of the sizable amount of data obtained in this study is shown in Fig. 5, which is a plot of the fusion temperature vs the crystal diameters for some representative samples. Also shown in Fig. 5 is the curve obtained from a least-squares fit to the second-order relations using all of the experimental points. The adjustable parameters are functions of γ_s and $\partial\gamma_s/\partial T$. When the experimental values summarized in Table I are employed, it is possible to calculate the surface tension of solid gold as $\gamma_s = 1.409 \pm 0.03 \text{ J m}^{-2}$, and to calculate its variation with respect to temperature as $\partial\gamma_s/\partial T = -2.64 \times 10^{-4} \pm 1 \times 10^{-4} \text{ J m}^{-2} \text{ }^\circ\text{K}^{-1}$. These values can be compared with those obtained by Buttner *et al.*³⁶ when extrapolated to the fusion temperature, $\gamma_s = 1.38 \pm 0.07 \text{ J m}^{-2}$ and $\partial\gamma_s/\partial T = -4.4 \times 10^{-4} \text{ J m}^{-2} \text{ }^\circ\text{K}^{-1}$. The result given by the Eötvös straight line is³⁶ $\partial\gamma_s/\partial T = -3.5 \times 10^{-4} \text{ J m}^{-2} \text{ }^\circ\text{K}^{-1}$.

It should be noted that a calculation made using

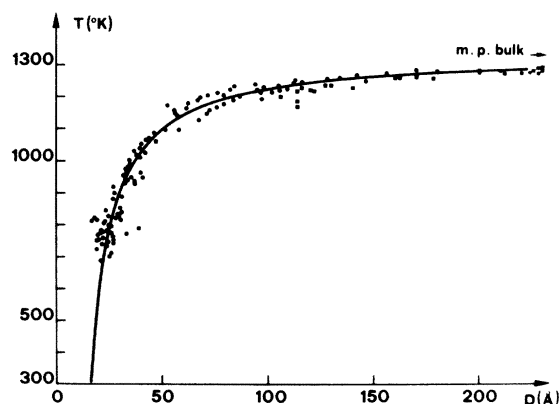


FIG. 5. Experimental and theoretical values of the melting-point temperature of gold particles: circles, present work; squares, Sambles (Ref. 28); the solid line results from a least-squares fit to the second-order relations of the first model, Eq. (13), using all the experimental data of the present work and an estimated value of the Debye-Waller factor.

our values for γ_s and $\partial\gamma_s/\partial T$ in the second-order thermodynamic approximation predicts that particles with a diameter of 20 Å will melt at a temperature of 600 °K. Although this approximation does not purport to apply exactly at temperatures which are quite different from the fusion temperature of the bulk material, the above result suggests that the estimate of the Debye-Waller factor might possibly be impaired by the fusion of the smallest crystals in the sample. For this reason, an additional type of analysis was applied to our experimental results. We assumed that the second-order theory was valid to temperatures as low as 350 °K,

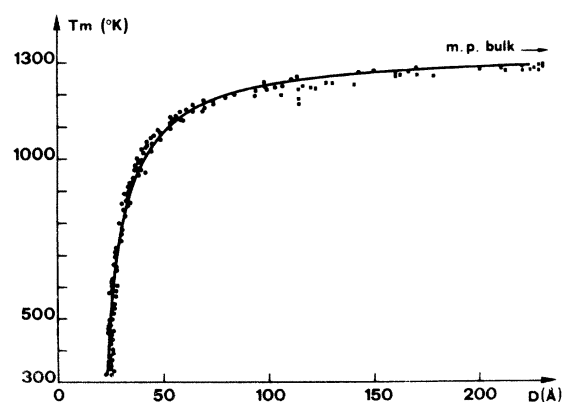


FIG. 6. Experimental and theoretical values of the melting-point temperature of gold particles, assuming validity of the first model in order to calculate the diffracted intensities and obtain the Debye-Waller factors: circles, present work; squares, Sambles (Ref. 28); the solid line results from a least-squares fit to Eq. (13) using all of the experimental points.

and calculated the variation of the integrated intensity starting from the mass distribution over the sample. This calculation was carried out using Eqs. (13), (21), and (22) and an analytical formulation of the size distributions in the samples.²⁹ The best fit of the theoretical predictions to the experimental data (see Fig. 6) occurs for the values $\gamma_s = 1.378 \text{ J m}^{-2}$ and $\partial\gamma_s/\partial T = -4.407 \times 10^{-4} \text{ J m}^{-2} \text{ }^\circ\text{K}^{-1}$, which are in excellent agreement with the values found by Buttner *et al.* It should be noted that the values of the Debye-Waller factor obtained on samples whose size distributions differed were quite independent of the particle diameters.²⁹ The dispersion of these values around the bulk value is within the limits of the experimental error. This result is in near agreement with measurements performed by Schroer *et al.*³⁷ who, using the Mössbauer effect, found the Debye-Waller factor of gold to be slightly dependent on the crystal sizes.

B. Comparison of results with the second phenomenological model

The results of the present work have also been compared with the predictions of the liquid-layer phenomenological model which was mentioned in Sec. III. In this case, the relation given in Eq. (18), which describes the system equilibrium, is essentially analytically close to Eq. (13), which is associated with the first model (to second order). The constants in the two equations, however, do not have the same physical significance. In the following discussion the particle radius will be denoted by r_s and the layer thickness by δ (with both quantities in units of meters). The interfacial tension will be expressed in J m^{-2} . For the case of gold particles, the two models successively lead to the expressions

$$r_s^2(\Theta - 1) + r_s[3.41 \times 10^{-10} - 7.01 \times 10^{-10}(\Theta - 1)] + 2.9 \times 10^{-21} = 0 \quad (24)$$

and

$$r_s^{*2} \ln \Theta + r_s^* [1.69 \times 10^{-9} \gamma_{st} - 1.25 \times 10^{-10} - 0.979 \delta \ln \Theta] + 1.22 \times 10^{-10} \delta = 0. \quad (25)$$

Both equations are seen to bear a close resemblance, since $\ln \Theta \approx \Theta - 1$ for T close to T_0 .

Since the liquid-layer model contains the layer thickness δ and the interfacial tension γ_{st} as adjustable parameters, both these quantities can be assigned numerical values which provide the best agreement with the experimental results. A method similar to the second type of analysis described in the preceding paragraph was used [utilizing Eq. (18)] with a relation which replaced

Eq. (23) and took into account the existence of a liquid layer in each particle. In this case the best fit to the experimental data was obtained for the values $\delta = 6.2 \text{ \AA}$ and $\gamma_{st} = 0.266 \text{ J m}^{-2}$. Figure 7 allows a comparison between the results obtained by successive use of the first and the second phenomenological models.

VIII. DISCUSSION

In order to treat the implications of these results, it is desirable to first discuss some of the features pertinent to the structure of small particles. The equilibrium shape for a perfect crystal is given by the Curie-Wulff relationship $\gamma_i/h_i = ct$, which leads, in turn, to the well-known construction of the “ γ plot.”^{38,39} It has been shown by some authors, however, that for small crystals, the existence of a multiple-twinned structure may produce particles whose energy is less than that of a Curie-Wulff crystal. (We shall hereafter denote “multiple twinned particles” by MTP.) For fcc structures, the predicted shapes are decahedrons or icosahedrons, which correspond to an arrangement of five tetrahedrons sharing a common edge or 20 tetrahedrons which have one vertex in common. In both these cases, the outermost faces of the particle are compact (111) surfaces whose surface tension is a minimum. In electron microscopy this type of particle appears to have practically spherical shapes for sizes inferior to 100 \AA . The changes in the diffraction contrast occurring between dark- and bright-field micrographs, however, make it possible to ascertain the presence

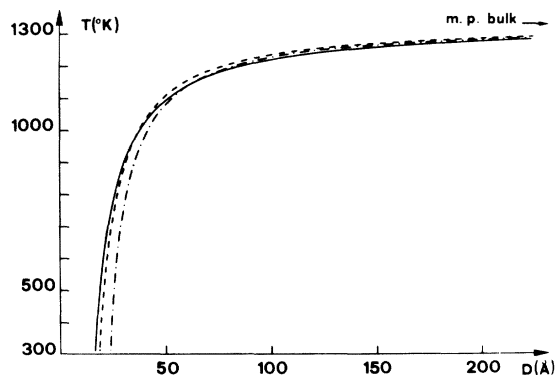


FIG. 7. Comparison of the various results obtained by successive use of the first and the second models. Solid line, first model to second-order, using an estimated Debye-Waller factor; dashed-and-dotted line, first model to second order, assuming validity of Eq. (13), in order to obtain an estimate of the Debye-Waller factor; dashed line, second model and Eq. (18), using the same estimate of the Debye-Waller factors as in the case of the solid line.

of multiple twins in small metallic particles. It therefore appears reasonable to replace the quantity γ_i/h_i by a term γ_s/r_s in the phenomenological calculations. [Here γ_s is the surface tension of the (111) faces and r_s is the solid-particle radius.] A more exact approximation would involve the energy of both twins as well as the deformation energy due to the presence of the twins. (Presumably this could have the effect of slightly modifying the latent heat of fusion and therefore the fusion temperature.) In order to retain a meaning for the concept of the critical temperature of fusion, one should, at least, assume that the particle microstructure is well-defined and invariant. The experimental findings of Sambles, who used electron microscopy to observe the behavior of a set of approximately similar particles lends support to the above criteria. Sambles was able to measure a unique temperature of fusion for each particle diameter within the limits of experimental error. This result is also in agreement with the work of Ino and Ogawa^{40,41} and Solliard *et al.*,⁴² which demonstrated the stability of the MTP shapes in the size range studied.

In contradistinction with the above results, Peppiat,¹⁴ who studied Pb crystals with diameters greater than 200 Å, found a dispersion in the values of the fusion temperature for a given diameter. It is possible that this effect is associated with the presence of defects in the crystals.

The micrographs do show that they contain twins and stacking faults. In his article, Peppiat does not specify whether or not these defects are related to well-defined MTP structures. Additionally, it should be noted that his study was necessarily limited to a group of well-faceted crystals. Although we are not able to disprove that a similar phenomenon might originate from imperfections in the MTP structure, we can ascertain that it does not influence the fusion temperature to within the limits of experimental error.

In summary, our experimental results are found to agree closely with the predictions of the first phenomenological model, provided that the physical constants for gold are the known values appropriate to the massive metal and that the surface tension of the solid phase is equal to the value determined by Buttner *et al.*³⁶ It should be noted that this latter value was measured on the cylindrical surface of a stretched wire and not on compact faces. Since the surface tension is only very weakly dependent on the face indices and since the low-indexed planes are the most developed, this does not raise any serious objections which could affect our results.

Our results also agree satisfactorily with the predictions of the second phenomenological model, provided the parameter δ is given the value of 6.2 Å and the interfacial tension a value of 0.266 Jm⁻². Thus our measurements do not permit a

TABLE I. Numerical values. Unless otherwise stated, the values have been assigned in this work to the physical constants of massive gold near the melting point.

	Solid	Liquid
Specific gravity ρ (kgm ⁻³)	18 400 (Ref. 12)	17 280 (Ref. 12)
Surface tension (between the condensed phases and the vapor) γ (Jm ⁻²)	1.38 (Ref. 36)	1.135 (Ref. 12)
$\frac{\partial \gamma}{\partial T}$ (Jm ⁻² °K ⁻¹)	-4.33×10^{-4} (Ref. 36)	-1.0×10^{-4} (Ref. 47)
Linear expansion coef. α (°K ⁻¹)	2.87×10^{-5} (Ref. 48)	2.25×10^{-5} (Ref. 49)
Isothermal compressibility coefficient χ (m ² N ⁻¹)	-5.99×10^{-12} (Ref. 33)	...
Specific heat at constant pressure, C_p (Jkg ⁻¹ °K ⁻¹)	169.2 (Ref. 50)	169.2 (Ref. 50)
Latent heat of fusion, L (Jkg ⁻¹)		6.27×10^4 (Ref. 12)
Melting point for the massive metal, T_0 (°K)		1336 (Ref. 12)
Interfacial tension (between solid and liquid phases) γ_{sl} (Jm ⁻²)		0.270 (Ref. 12)
Liquid layer thickness δ (Å)		22 (Ref. 12)

conclusive choice to be made between the two models. The crucial element required for such a distinction is an experiment which could prove or disprove, for the case of gold, the existence of a liquid surface layer.

Goodman and Somorjai⁴³ have investigated the melting point of faces with low Miller indices in massive monocrystals of Pb, Bi, and Sn using a LEED technique and concluded that the surface and the volume melting points were equivalent. The experiments which show the complete fusion of a very thin layer deposited on a distinct substrate⁴⁴ should, however, be clearly distinguished from this measurement of the surface melting temperature on a massive solid. Additionally Sundquist¹⁶ has produced evidence in the case of silver for a critical temperature at which the surface tension becomes isotropic. He attributed this result to the existence of a surface roughness as introduced by Burton *et al.*⁴⁵ This phenomenon does not appear to be equivalent to the formation of an actual liquid layer and would be better described by the well-known superficial layer model of Van der Waals, Jr. and Backer. Defay⁴⁶ has shown the thermodynamical equivalence at equilibrium between the latter model and the Gibbs surface model which we have been using.

Thus, to our knowledge, and in the case of metals, no direct evidence establishing the existence, below the melting point, of a liquid layer

which exhibits the properties associated with the second phenomenological model can be found in the literature. Although this situation does not favor the liquid-layer model, it is possible that the existence of such a liquid layer is itself dependent on a size effect. If this is the case, however, it would appear to be unlikely that the thickness would be independent of both the particle diameter and the temperature.

ACKNOWLEDGMENTS

We wish to thank Professor Ch. Gruber for his valuable remarks concerning the thermodynamic calculations, and Professor J. Buttet, Dr. L. A. Boatner, and Dr. J-P. Heger for their comments while reviewing the manuscript and the active part they took in its translation. We would like to express our appreciation to J. D. Ganière for a Fortran program to interpret the experimental data within the framework of the liquid-layer model, and to J. C. Lecomte who, as an undergraduate student, was first concerned with the experimental technique described above. The technical facilities of the Interdepartmental Institute of Metallurgy of the Federal Institute of Technology-Lausanne were obligingly made available to us.

*Work was supported by the Swiss National Fund for Scientific Research under Grants 2.1940.74 and 2.8860.73.

¹M. R. Hoare and P. Pal, *J. Cryst. Growth* **17**, 77 (1972).

²J. G. Allpress and J. V. Sanders, *Aust. J. Phys.* **23**, 23 (1970).

³M. Takagi, *J. Phys. Soc. Jpn.* **9**, 359 (1954).

⁴M. Blackman and A. E. Curzon, *Structure and Properties of Thin Films* (Wiley, New York, 1959), p. 217.

⁵C. R. M. Wronski, *Br. J. Appl. Phys.* **18**, 1731 (1967).

⁶C. J. Coombes, *J. Phys.* **2**, 441 (1972).

⁷N. T. Gladkikh, R. Niedermayer, and K. Spiegel, *Phys. Status Solidi* **15**, 181 (1966).

⁸B. T. Boiko, A. T. Pugachev, and V. M. Bratsykhin, *Fiz. Tverd. Tela* **10**, 3567 (1968) [*Sov. Phys.-Solid State* **10**, 2832 (1969)].

⁹J. F. Pocza, A. Barna, and P. B. Barna, *J. Vac. Sci. Technol.* **6**, 472 (1969).

¹⁰R. P. Berman and A. E. Curzon, *Can. J. Phys.* **52**, 923 (1974).

¹¹Yu. I. Petrov and V. A. Kotelnikov, *Phys. Status Solidi* **34**, K123 (1969).

¹²J. R. Sambles, *Proc. R. Soc. A* **324**, 339 (1971).

¹³J. R. Sambles, L. M. Skinner, and N. D. Lisingarten, *Proc. R. Soc. A* **318**, 507 (1970).

¹⁴S. J. Peppiatt, *Proc. R. Soc. A* **345**, 387 (1975); **345**, 401 (1975).

¹⁵M. Blackman, S. J. Peppiatt, and J. R. Sambles, *Nat. Phys. Sci.* **239**, 61 (1972).

¹⁶B. E. Sundquist, *Acta Metall.* **12**, 585 (1964).

¹⁷B. E. Sundquist, *Acta Metall.* **12**, 67 (1964).

¹⁸H. M. Kennett, A. E. Lee, and J. M. Wilson, *Proc. R. Soc. A* **331**, 429 (1972).

¹⁹R. Defay, I. Prigogine, A. Bellemans, and D. H. Everett, *Surface Tension and Adsorption* (Longmans, Green, London, 1966), p. 286.

²⁰N. D. Lisingarten, J. R. Sambles, and L. M. Skinner, *Contemp. Phys.* **12**, 575 (1971).

²¹V. K. La Mer and R. Gruen, *Trans. Faraday Soc.* **48**, 410 (1952).

²²F. Piuz and J-P. Borel, *Phys. Status Solidi A* **14**, 129 (1972).

²³P. Pawlow, *Z. Phys. Chem.* **65**, 1 (1909); **65**, 545 (1909).

²⁴K-J. Hanszen, *Z. Phys.* **157**, 523 (1960).

²⁵J-P. Borel, *C. R. Acad. Sci. C* **227**, 1275 (1973).

²⁶H. Reiss and I. B. Wilson, *J. Colloid Sci.* **3**, 551 (1948).

²⁷R. Defay, *et al.*, Ref. 19, p. 313.

²⁸J. R. Sambles, Ph.D. thesis (University of London, London, 1970) (unpublished).

²⁹Ph. Buffat, Ph.D. thesis (Ecole Polytechnique Fédérale - Lausanne, 1976) (unpublished).

³⁰*Handbook of Chemistry and Physics*, edited by R. C. Weast (Chemical Rubber Publishing Co., Cleveland,

- Ohio, 1971), 52nd ed., p. E207.
- ³¹B. K. Vainshtein, *Structure Analysis by Electron Diffraction* (Pergamon, New York, 1964), p. 141.
- ³²T. B. Rymer, *Electron Diffraction* (Methuen, London, 1970), p. 106.
- ³³C. W. Mays, J. S. Vermaak, and D. Kuhlmann-Wilsdorf, *Surf. Sci.* **12**, 134 (1968).
- ³⁴D. C. Smart, F. W. Boswell, and J. M. Corbett, *J. Appl. Phys.* **43**, 4461 (1972).
- ³⁵Ph. Buffat, *Thin Solid Films* **32**, 283 (1975).
- ³⁶H. Buttner, H. Udin, and J. Wulff, *J. Met. Trans. AIME* **3**, 1209 (1951); **4**, 401 (1952).
- ³⁷D. Schroeer, R. F. Marzke, D. J. Erikson, S. W. Marshall, and R. M. Wilenzick, *Phys. Rev. B* **2**, 4414 (1970).
- ³⁸C. Herring, *Structure and Properties of Solid Surfaces* (University of Chicago, Chicago, 1952), p. 24.
- ³⁹W. W. Mullins, *Metal Surfaces: Structure Energetics, and Kinetics* (American Society for Metals, Ohio, 1962), p. 28.
- ⁴⁰S. Ino and S. Ogawa, *J. Phys. Soc. Jap.* **22**, 1365 (1967).
- ⁴¹S. Ogawa and S. Ino, *J. Vac. Sci. Technol.* **6**, 527 (1969).
- ⁴²C. Solliard, Ph. Buffat, and F. Faes, *J. Cryst. Growth* **32**, (1976).
- ⁴³R. M. Goodman and G. A. Somorjai, *J. Chem. Phys.* **52**, 6325 (1970).
- ⁴⁴J. Henrion and G. E. Rhead, *Surf. Sci.* **29**, 20 (1972).
- ⁴⁵W. K. Burton, N. Cabrera, and F. C. Frank, *Philos. Trans. R. Soc. A* **243**, 299 (1951).
- ⁴⁶R. Defay *et al.*, Ref. 19, pp. 21 and 386.
- ⁴⁷V. K. Semenchenko, *Surface Phenomena in Metals and Alloys* (Pergamon, New York, 1961), p. 403.
- ⁴⁸*American Institute of Physics Handbook*, 3rd ed. (McGraw-Hill, New York, 1972), pp. 4-124.
- ⁴⁹Reference 30, 52nd ed., p. B235.
- ⁵⁰*Selected Values of the Thermodynamic Properties of the Elements* (American Society for Metals, Ohio, 1973), p. 50.